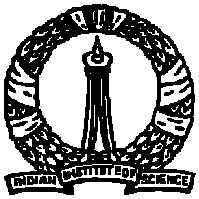

AR&DB Centre of Excellence for Aerospace CFD
Department of Aerospace Engineering
Indian Institute of Science

Fluid Mechanics Report

Low Dissipative Modified KFVS (M-KFVS) Method

N Anil
AR&DB Centre of Excellence for Aerospace CFD
Department of Aerospace Engineering
Indian Institute of Science
Bangalore 560012

SM Deshpande
Engineering Mechanics Unit
Jawaharlal Nehru Centre for Advanced Scientific Research
Jakkur, Bangalore 560064

Report 2004 FM 22
November 2004

Fluid Mechanics Report

Low Dissipative Modified KFVS (M-KFVS) Method

N Anil

AR&DB CFD Centre,
Department of Aerospace Engg.,
Indian Institute of Science,
Bangalore 560012, India
Email: anil@aero.iisc.ernet.in

SM Deshpande

Engineering Mechanics Unit,
Jawaharlal Nehru Centre for Advanced Scientific Research,
Bangalore 560064, India
Email: smd@jncasr.ac.in

1 Introduction

Kinetic theory based schemes belong to the family of upwind schemes and have been demonstrated to be very robust and efficient in solving problems of practical interest [2, 3, 18, 26]. These schemes are based on the moment-method-strategy [7] where an upwind scheme is developed at the Boltzmann level and taking moments we arrive at an upwind scheme for the conservation laws of gas dynamics. Exploiting the above connection between the Boltzmann equation and the Euler equations, various kinetic theory based numerical schemes [14, 15, 16, 17, 19, 21, 25] have been developed. The *kfvs* scheme developed by Mandal and Deshpande [14] is one of the earliest schemes of its kind.

The usual first order kinetic scheme is found to be more dissipative. However, higher order accurate schemes have been constructed for better accuracy and for considerably reducing numerical dissipation. To control the dissipation in the first order *kfvs* scheme, Deshpande[22] has defined a modified way of CIR splitting, namely MCIR splitting of the molecular velocity by introducing a dissipation control function. Using the above idea and with different mathematical models for the dissipation control function, many numerical schemes [8, 10, 22] have been developed recently.

In the present work we construct a modified *kfvs* (*m-kfvs*) scheme based on MCIR splitting with molecular velocity dependent dissipation control functions. Section 2 presents the basics of first order *kfvs* scheme. The modified CIR (MCIR) splitting is described in Section 3.1. The limit in which the kinematic numerical viscosity based on MCIR splitting becomes zero and the limit in which usual *kfvs* is obtained have been studied in details. Section 3.2 presents the different choices for the dissipation control function and their behaviour in great detail. The expressions for the *m-kfvs* fluxes are derived in section 3.3. The corresponding numerical scheme based on finite volume discretisation is presented in section 4.

Section 5 presents the results obtained using *m-kfvs* scheme on standard test cases for one dimensional flows. Numerical results obtained for the shock tube problem show that the *m-kfvs* method resolves the discontinuties more sharply and is less dissipative. Solutions for the nozzle problem are in good comparison with MacCormack scheme. The *m-kfvs* method with proper tuning of dissipation control function gives near second order accuracy in smooth regions as well as captures the discontinuties very crisply without spurious oscillations.

The *m-kfvs* scheme can be easily extended to higher dimensions. The expressions for the split fluxes for $2D$ and $3D$ flows are presented in *Appendix A*. Infact, the above idea can be easily incorporated into the existing $2D$ and $3D$ codes based on *kfvs*, just by modifying the expressions for the split fluxes.

2 A brief description of kfvs

In this section we illustrate the basic principles of kinetic flux vector split (*kfvs*) scheme [6, 14] with reference to 1D unsteady Euler equations given by

$$\frac{\partial U}{\partial t} + \frac{\partial G}{\partial x} = 0 \tag{1}$$

where U is the vector of conserved variables and G is the flux vector. The above system of equations can be obtained by taking the Ψ - moments of the $1D$ Boltzmann equation in the Euler limit

$$\frac{\partial F}{\partial t} + \frac{\partial (vF)}{\partial x} = 0 \tag{2}$$

where F is the Maxwellian velocity distribution function given by

$$F = \frac{\rho}{I_0}\sqrt{\frac{\beta}{\pi}} \exp\left[-\beta(v-u)^2 - I/I_0\right] \tag{3}$$

Here, ρ density, v molecular velocity, u fluid velocity, I internal energy variable, R gas constant per unit mass, $\beta = \frac{1}{2RT}$, I_0 internal energy due to nontranslational degrees of freedom, given by

$$I_0 = \frac{3-\gamma}{4(\gamma-1)\beta}$$

The moment function vector Ψ is defined by

$$\Psi = \begin{bmatrix} 1 \\ v \\ I + \frac{v^2}{2} \end{bmatrix}$$

The Euler equations (1) can then be written as

$$\frac{\partial U}{\partial t} + \frac{\partial G}{\partial x} = \left\langle \Psi, \frac{\partial F}{\partial t} + \frac{\partial (vF)}{\partial x} \right\rangle = 0 \tag{4}$$

where $U = \langle \Psi, F \rangle$, $G = \langle \Psi, vF \rangle$ and the inner product $\langle \Psi, f \rangle$ is defined by

$$\langle \Psi, f \rangle = \int_{\mathbb{R}^+ \times \mathbb{R}} \Psi f(v) dv dI \tag{5}$$

Using CIR splitting [5], eq. 2 gives a semidiscretised upwind scheme for the $1D$ Boltzmann equation,

$$\left(\frac{\partial F}{\partial t}\right)_j + \frac{v+|v|}{2}\frac{F_j - F_{j-1}}{\Delta x} + \frac{v-|v|}{2}\frac{F_{j+1} - F_j}{\Delta x} = 0 \tag{6}$$

Taking the Ψ - moments of the above equation with a forward difference approximation to the time derivative, we arrive at an upwind scheme for the $1D$ Eluer equations,

$$U_j^{n+1} = U_j^n - \Delta t \left[\frac{G_j^+ - G_{j-1}^+}{\Delta x} + \frac{G_{j+1}^- - G_j^-}{\Delta x} \right]^n \tag{7}$$

where $G^{\pm}$ are the *kfvs* fluxes, and are given by

$$G^{\pm} = \left\langle \Psi, \frac{v \pm |v|}{2} F \right\rangle = \int_{\mathbb{R}^+ \times \mathbb{R}^{\pm}} \Psi v F dv dI \tag{8}$$

Using Taylor series, eq. (6) gives the modified partial differential equation (mpde),

$$\frac{\partial F}{\partial t} + v\frac{\partial F}{\partial x} = \frac{\Delta x}{2}|v| F_{xx} + O\left(\Delta x^2\right) \tag{9}$$

In the above equation the leading term in the truncation error is of the order of $O(\Delta x)$, showing that the upwind scheme (6) using CIR splitting is first oder accurate and is dissipative.

We pose the following questions. Is there any mechanism through which we can have a direct control over the numerical dissipation ? Is it possible to develop a numerical scheme with nearly second order accuracy in smooth regions and capturing the discontinuties sharply without wiggles ? Of course, this question has been the subject of research for about two decades and we ask this question in the framework of kinetic schemes.

In the next section, we present modified way of CIR splitting by introducing a dissipation control function, through which we can address the above questions.

3 Basics of m-kfvs

3.1 MCIR splitting

The mpde (9) corresponding to the semidiscretised Boltzmann equation (6) shows that $|v|$ contributes to the numerical dissipation. To reduce the numerical dissipation, Deshpande [23] has introduced a dissipation control function ϕ as a multiplying factor for $|v|$. The modified way of CIR splitting of the molecular velocity, called MCIR splitting [22, 23] is given by

$$v = v^+ + v^- = \frac{v + |v|\phi}{2} + \frac{v - |v|\phi}{2} \tag{10}$$

Using the above defined MCIR splitting, the $1D$ Boltzmann equation (2) reduces to

$$\frac{\partial F}{\partial t} + \frac{\partial}{\partial x}\left(\frac{v + |v|\phi}{2}F\right) + \frac{\partial}{\partial x}\left(\frac{v - |v|\phi}{2}F\right) = 0 \tag{11}$$

and the corresponding semidiscrete upwind scheme is given by

$$\left(\frac{\partial F}{\partial t}\right)_j + \frac{v + |v|\phi}{2}\frac{F_j - F_{j-1}}{\Delta x} + \frac{v - |v|\phi}{2}\frac{F_{j+1} - F_j}{\Delta x} = 0 \tag{12}$$

The mpde analysis of the above equation gives

$$\frac{\partial F}{\partial t} + v\frac{\partial F}{\partial x} = \frac{\Delta x}{2}|v|(\phi F)_{xx} + O\big(\Delta x^2\big) \tag{13}$$

Taking the Ψ - moments, we arrive at

$$\frac{\partial U}{\partial t} + \frac{\partial G}{\partial x} = \frac{\Delta x}{2}\int\limits_{\mathbb{R}^+\times\mathbb{R}} \Psi|v|(\phi F)_{xx}dvdI + O\big(\Delta x^2\big) \tag{14}$$

In terms of ϕ the modified split fluxes are easily defined as

$$Gm^{\pm} = \int\limits_{\mathbb{R}^+\times\mathbb{R}} \frac{v \pm |v|\phi}{2}\Psi F dvdI \tag{15}$$

Obviously, from (14) as well as (15) it follows that $\phi = 1$ gives $Gm^{\pm} = G^{\pm}_{kfvs}$, the usual *kfvs* fluxes, while $\phi = 0$ leads to a central difference scheme. Let us explain this aspect further. Consider the semidiscrete Boltzmann equation obtained in eq. (12),

$$\left(\frac{\partial F}{\partial t}\right)_j + \frac{v + |v|\phi}{2}\frac{F_j - F_{j-1}}{\Delta x} + \frac{v - |v|\phi}{2}\frac{F_{j+1} - F_j}{\Delta x} = 0 \tag{16}$$

which can be cast in the Finite Volume Method (FVM) as

$$\left(\frac{\partial F}{\partial t}\right)_j + \frac{1}{\Delta x}\left\{\left(\frac{v + |v|\phi}{2}F_j + \frac{v - |v|\phi}{2}F_{j+1}\right) - \left(\frac{v - |v|\phi}{2}F_j + \frac{v + |v|\phi}{2}F_{j-1}\right)\right\} = 0 \tag{17}$$

Taking the Ψ - moments yield the semidiscrete conservation law for the Euler equations as

$$\left(\frac{\partial U}{\partial t}\right)_j + \frac{G_{j+\frac{1}{2}} - G_{j-\frac{1}{2}}}{\Delta x} = 0 \tag{18}$$

where

$$\begin{aligned} G_{j+\frac{1}{2}} &= \int\limits_{\mathbb{R}^+\times\mathbb{R}} \left(\frac{v + |v|\phi}{2}F_j + \frac{v - |v|\phi}{2}F_{j+1}\right)\Psi dvdI \\ G_{j-\frac{1}{2}} &= \int\limits_{\mathbb{R}^+\times\mathbb{R}} \left(\frac{v + |v|\phi}{2}F_{j-1} + \frac{v - |v|\phi}{2}F_j\right)\Psi dvdI \end{aligned} \tag{19}$$

It is very evident that $\phi = 0$ leads to central differencing and $\phi = 1$ gives the normal *kfvs* scheme. Let us analyse the formulae in (19) further. We write $G_{j+\frac{1}{2}}$ in the form

$$G_{j+\frac{1}{2}} = \int\limits_{\mathbb{R}^+\times\mathbb{R}} \left(v\frac{F_j + F_{j+1}}{2} - |v|\phi\frac{F_{j+1} - F_j}{2}\right)\Psi dvdI \tag{20}$$

from which we observe that $G_{j+\frac{1}{2}}$ can be considered as a flux of the velocity distribution function

$$F_{j+\frac{1}{2}} = \frac{F_j + F_{j+1}}{2} - sgn(v)\phi\frac{F_{j+1} - F_j}{2} \tag{21}$$

A switching function appears in the definition of $F_{j+\frac{1}{2}}$ and because of it $F_{j+\frac{1}{2}} = F_j$ when $v > 0$ and $F_{j+\frac{1}{2}} = F_{j+1}$ when $v < 0$ provided $\phi = 1$. The modified *kfvs* fluxes (19) which are the Ψ - moments of (21) contain the weight function $\phi(v)$ multiplying the switch. This is reminiscent of the "addition of controlled diffusion" approach pioneered by Jameson [11].

Thus, by tuning ϕ such that $0 < \phi \leq 1$ we can control the numerical dissipation and hence order of accuracy. Infact, Ramesh and Deshpande [22, 23] have assumed $\phi = k|\Delta x|^p$, $0 \leq p < 1$, and obtained an accuracy of $(\Delta x)^{p+1}$ although the formal order of accuracy being first order if ϕ is assumed to be independent of Δx. Numerical experiments of Ramesh and Deshpande [22, 23] are very interesting. These computations reveal that the way ϕ tends to zero is important from the point of view of stability. At exactly $\phi = 0$, the numerical scheme is unstable.

3.2 Mathematical models for ϕ

In this section we present different choices for the dissipation control function ϕ, which is a non linear function of molecular velocity v.
Consider the mpde obtained in the eq. (14). When $\Psi = 1$, the mpde corresponding to the mass balance equation is given by

$$\begin{aligned} \frac{\partial \rho}{\partial t} + \frac{\partial}{\partial x}(\rho u) &= \frac{\partial^2}{\partial x^2}\left[\frac{\Delta x}{2}\int\limits_{\mathbb{R}^+\times\mathbb{R}} |v|\phi\rho\sqrt{\frac{\beta}{\pi}}\frac{1}{I_0}e^{-\beta(v-u)^2 - I/I_0}dvdI\right] \\ &= \frac{\partial^2}{\partial x^2}\Big[\nu_{num}\rho\Big] \end{aligned} \tag{22}$$

where ν_{num} is the numerical kinetic viscosity given by

$$\nu_{num} = \frac{\Delta x}{2}\sqrt{\frac{\beta}{\pi}}\int\limits_{\mathbb{R}} |v|\phi e^{-\beta(v-u)^2}dv \tag{23}$$

From the above equation we observe that the absolute value of velocity, $|v|$ is multiplied by velocity dependent exponential in the integrand on RHS of eq. (23). For the case of $\phi = 1$, maximum contribution to the numerical viscosity comes from particles with velocities close to u, i.e., $c = v - u \approx 0$. Particles with large $|c|$ contribute very little to ν_{num}. If we can suitably weight the particles contributing maximum to ν_{num}, then we can reduce the numerical viscosity in the scheme. The control function ϕ plays this role. Obviously, ϕ must be a function of molecular velocity v to achieve the objective, that is, to reduce ν_{num}. We have considered two choices,

$$\phi = e^{-\frac{\alpha}{|v|}} \qquad \text{and} \qquad \phi = e^{-\alpha|v|} \tag{24}$$

where α could be a mesh dependent function, which we will define later. For both the choices, ϕ is an exponentially decaying function. Also, in the limit $\alpha \to 0 \Rightarrow \phi = 1$ and $\alpha \to \infty \Rightarrow \phi = 0$, resulting in first order accurate *kfvs* and central differencing schemes respectively.

When $\phi = e^{-\frac{\alpha}{|v|}}$, the control function ϕ is very small for particles with $|v|$ close to zero. Thus low velocity particles are not allowed to contribute significantly to ν_{num}. For $|v| \to \infty$, $\phi \to 1$ and contribution to numerical viscosity comes from high velocity particles whose number density is very small due to Gaussian distribution. Fig. 1(a) shows the effect of this model on the kinematic numerical viscosity, ν_{num}. The parameter α is a characteristic velocity scale of the control function and low and high ends of $|v|$ are controlled by α. We can introduce non-dimensional control parameter $\tilde{\alpha}$ as

$$\alpha = \tilde{\alpha}/\sqrt{\beta} \tag{25}$$

The other choice for control function is $\phi = e^{-\alpha|v|}$. In this case low velocity particles, that is, particles for which

$$\alpha|v| \ll 1, \quad \text{or} \quad |v| \ll \frac{1}{\alpha} \tag{26}$$

contribute most to ν_{num}. Obviously, particles for which

$$\alpha|v| \gg 1, \quad \text{or} \quad |v| \gg \frac{1}{\alpha} \tag{27}$$

will contribute very little to kinematic numerical viscosity. The corresponding behaviour of ν_{num} using $\phi = e^{-\alpha|v|}$ is shown in Fig. 1(b). Again, α^{-1} is a characteristic scale of the weighting function $e^{-\alpha|v|}$. Thus, it is possible to weight the velocity space suitably for reducing the dissipation. We now demonstrate the effect of these choices on the behaviour of v^+ and v^-.

Using the choice $\phi = e^{-\frac{\alpha}{|v|}}$*:*

In this case we discuss several possibilities depending on the value of $\frac{\alpha}{|v|}$.

1. Those particles for which $\frac{\alpha}{|v|} \gg 1$, we get $e^{-\frac{\alpha}{|v|}} \simeq 0$ and hence the value of v^+ is given by

$$v^+ \simeq \frac{v}{2} \tag{28}$$

2. When $\frac{\alpha}{|v|} \simeq 1$, then $e^{-\frac{\alpha}{|v|}} \simeq e^{-1}$ and in this case v^+ is given by

$$v^+ = \begin{cases} \frac{v(e+1)}{2e} & \text{for } v > 0 \\ \frac{v(e-1)}{2e} & \text{for } v < 0 \end{cases} \tag{29}$$

3. When $\frac{\alpha}{|v|} \ll 1$, we obtain $e^{-\frac{\alpha}{|v|}} \simeq 1$ and hence $v^+ \simeq \frac{v+|v|}{2}$.

It is evident that all the particles for which $\frac{\alpha}{|v|} \gg 1$ contribute a lot to the downwind effect. Fig. 2(a) shows the behaviour of v^+ for small and large values of α.

The choice $\phi = e^{-\alpha|v|}$*:*

In this case all those particles for which

1. $\alpha|v| \ll 1$, we have $e^{-\alpha|v|} \simeq 1$ and hence the value of v^+ is given by

$$v^+ \simeq \frac{v + |v|}{2} \tag{30}$$

2. $\alpha|v| \gg 1$, then we have $e^{-\alpha|v|} \simeq 0$ and in this case v^+ is given by

$$v^+ \simeq \frac{v}{2} \tag{31}$$

Therefore, in this case it is the high velocity particles which are contributing most to the downwind effect, and the plot of v^+ with v is shown in Fig. 2(b). We can carry out similar arguments for the behaviour of v^- from Figs. 2(c) and 2(d). Also, we observe that, as the value of α increases the downwind effect increases further.

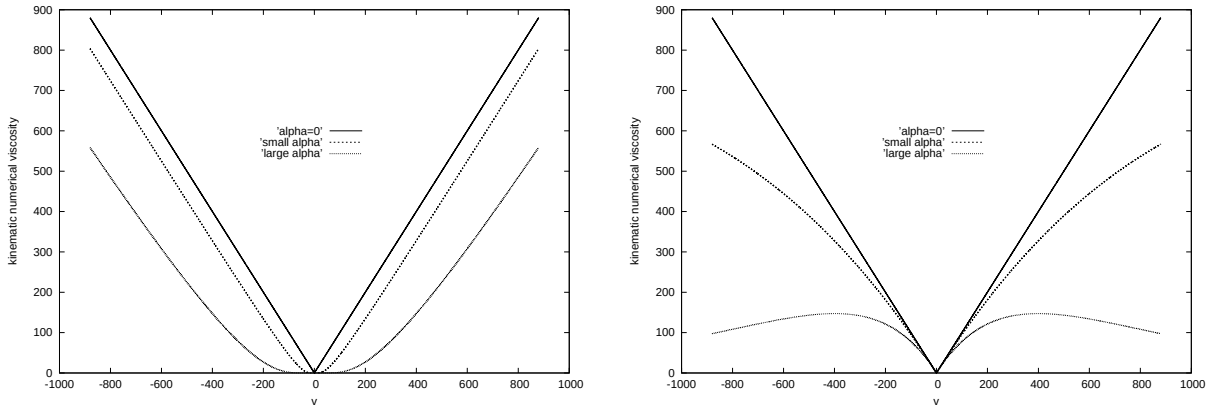

(a) $\phi = e^{-\frac{\alpha}{|v|}}$ (b) $\phi = e^{-\alpha|v|}$

Figure 1: Behaviour of the kinematic numerical viscosity for different models of ϕ.

Let us understand more about low and high velocity molecules. Consider the steady $1D$ Boltzmann equation with a BGK - model for the collision terms

$$v\frac{\partial f}{\partial x} = A(F - f) \tag{32}$$

Here, f is the velocity distribution function, A^{-1} the relaxation time scale and F the local Maxwellian velocity distribution function. Using the interating factor $e^{Ax/v}$ we can write the solution of (32) as

$$f(x,v) = f(x_0,v)e^{-\frac{A}{v}(x-x_0)} + \int_{x_0}^{x} \frac{A}{v}F(x')e^{\frac{A}{v}(x'-x_0)}dx', \quad v > 0 \tag{33}$$

Similar formula can be written down for $v < 0$, but that is not required for making the main point in the following argument. Assuming $F(x')$ to be a constant over the interval $x \leq x' \leq x_0$ (which is $\simeq \Delta x$), we get

$$f(x,v) = f(x_0,v)e^{-\frac{A}{v}(x-x_0)} + F\left[1 - e^{-\frac{A}{v}(x-x_0)}\right] \tag{34}$$

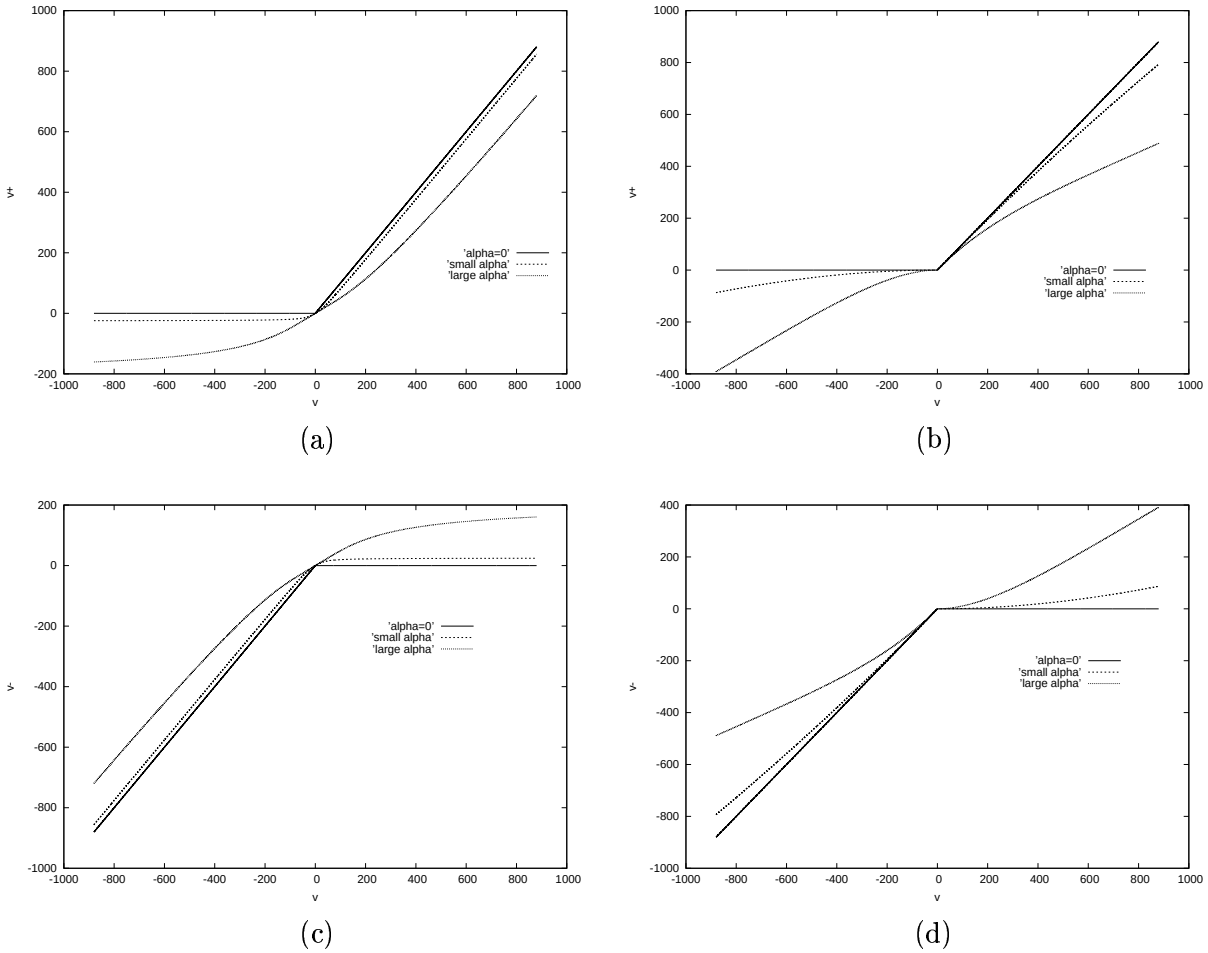

Figure 2: (a) and (b) show the behaviour of v^+ with respect to v when $\phi = e^{-\frac{\alpha}{|v|}}$ and $\phi = e^{-\alpha|v|}$ respectively, (c) and (d) show the corresponding behaviour of v^-.

It is clear from the above equation that the low velocity molecules are almost always lost (in the sense of loss term in the Boltzmann equation) while high velocity molecules are lost negligibly, that is, they travel over Δx without any collision. Therefore, it makes sense in using a weight function in velocity space which has the above property. The choice of $\phi = e^{-\frac{\alpha}{|v|}}$ is therefore consistent with the above physical argument. The second choice $\phi = e^{-\alpha|v|}$ leads to much simpler formulae for split fluxes and is shown in the next section. It is therefore interesting to study the *m-kfvs* (modified *kfvs*) method further by applying it to some examples.

3.3 m-kfvs fluxes

In this section we will derive closed form expressions for the split fluxes in the modified *kfvs* method. These split fluxes are denoted by $Gm^{\pm}$ and are given by

$$Gm^{\pm} = \left\langle \Psi, \frac{v \pm |v|\phi}{2} F \right\rangle \tag{35}$$

We have used two models $\phi = e^{-\frac{\alpha}{|v|}}$ and $\phi = e^{-\alpha|v|}$, discussed in the previous section.

3.3.1 The first model, $\phi = e^{-\frac{\alpha}{|v|}}$:

The expressions for the *m-kfvs* split fluxes using the first choice $\phi = e^{-\frac{\alpha}{|v|}}$ are given by

$$\begin{aligned} Gm^{\pm} &= \left\langle \Psi, \frac{v \pm |v| e^{-\frac{\alpha}{|v|}}}{2} F \right\rangle \\ &= \frac{1}{2} \int\limits_{\mathbb{R}^+ \times \mathbb{R}} \left[\Psi v F dv dI \pm \Psi |v| e^{-\frac{\alpha}{|v|}} F dv dI \right] \\ &= \frac{G}{2} \pm \frac{\rho}{2} \sqrt{\frac{\beta}{\pi}} \int\limits_{\mathbb{R}} \Psi |v| e^{-\beta(v-u)^2 - \frac{\alpha}{|v|}} dv \\ &= \frac{G}{2} \pm \frac{\rho}{2} \sqrt{\frac{\beta}{\pi}} \left[\int\limits_{-\infty}^{0} \Psi |v| e^{-\beta(v-u)^2 - \frac{\alpha}{|v|}} dv + \int\limits_{0}^{\infty} \Psi |v| e^{-\beta(v-u)^2 - \frac{\alpha}{|v|}} dv \right] \end{aligned} \tag{36}$$

On simplifying the integrals, the final exressions for the split fluxes are given by

$$Gm^{\pm} = \frac{G}{2} \pm \frac{\rho}{2} \sqrt{\frac{\beta}{\pi}} \begin{bmatrix} \frac{1}{\beta} \Big\{ J_1(A,S) + J_1(A,-S) \Big\} \\ \frac{1}{\beta^{3/2}} \Big\{ J_2(A,S) - J_2(A,-S) \Big\} \\ \frac{I_0}{\beta} \Big\{ J_1(A,S) + J_1(A,-S) \Big\} + \frac{1}{\beta^2} \Big\{ J_3(A,S) + J_3(A,-S) \Big\} \end{bmatrix} \tag{37}$$

where G is the unsplit flux and we have used the notation for the integral

$$\int\limits_{0}^{\infty} v^n e^{-\beta(v-u)^2 - \frac{\alpha}{v}} dv = \frac{1}{\beta^{(n+1)/2}} J_n(A,S) \tag{38}$$

The function $J_n(A,S)$ given in [4] is defined by

$$J_n(A,S) = \int\limits_{0}^{\infty} v^n e^{-(v-S)^2 - \frac{A}{v}} dv \tag{39}$$

where $A = \alpha\sqrt{\beta}$ and $S = u\sqrt{\beta}$. The function $J_n(A,S)$, $\forall A, S \in R$ and $A > 0$ is not in general reducible to any of the standard tabulated definite integrals because of the presence of

v as denominator in $\frac{A}{v}$ in the argument of the exponential. Also, numerical integration of the function is difficult and very expensive. However, depending on the value of A and S convergent series [1] and asymptotic expansions [4] of the integral $J_n(A,S)$ are available. Note that, the function $J_n(A,S)$ satisfies the recurrence relation

$$2J_n = 2SJ_{n-1} + (n-1)J_{n-2} + AJ_{n-3} \tag{40}$$

The case S=0:

In this case, for the function $J_n(A,0)$, Abramowitz [1] has given a series expansion suitable for small values of A and an asymptotic expansion for large values of A.

For small A

$$\begin{aligned} J_0(A,0) &= \frac{\sqrt{\pi}}{2} - S_0 \\ J_1(A,0) &= \frac{1}{2} - \frac{\sqrt{\pi}}{2}A + S_1 \\ J_2(A,0) &= \frac{\sqrt{\pi}}{4}(1+A^2) + \frac{A}{2} - S_2 \end{aligned} \tag{41}$$

For $n \geq 3$, we use the recurrence relation given by the eq. (40) and S_n is defined by

$$\begin{aligned} S_n = \sum_{r=0}^{\infty} \frac{(-1)^r \left[\frac{1}{2}\psi(r+1) + \psi(2r+2+n) - \log A\right]}{r!(2r+1+n)!} A^{2r+1+n} \\ + \sqrt{\pi} \sum_{r=0}^{\infty} \frac{(-2)^r A^{2r+2+n}}{1.3.5...(2n+1)(2r+2+n)!} \end{aligned}$$

For large A

$$J_n(A,0) \approx \left(\frac{\pi}{3}\right)^{\frac{1}{2}} \left(\frac{A}{2}\right)^{\frac{n}{3}} \left[a_0 + \frac{a_1(n)}{z} + \frac{a_2(n)}{z^2} + \frac{a_3(n)}{z^3} + ...\right] e^{-z} \tag{42}$$

where $z = 3\left(\frac{A}{2}\right)^{\frac{2}{3}}$. The values of a_0 and $a_1(n)$ are

$$a_0 = 1,\ a_1(n) = \frac{1}{12}(3n^2 + 3n - 1)$$

The recurrence relation for $a_i(n)$ is given by

$$\begin{aligned} 12(i+2)a_{i+2} = -(12i^2 + 36i - 3n^2 - 3n + 25)a_{i+1} \\ + \frac{1}{2}(n-2i)(3i+3-n)(3i+3+2n)a_i,\ i = 0,1,2,... \end{aligned}$$

The case $S \neq 0$:

In this case Chahine and Narasimha [4] had given asymptotic expansions for the function $J_n(A,S)$ based on large positive S, small positive S and negative S.

Large positive S

For large positive S, asymptotic expressions are available based on $X = A/S^3$ is small or large. However, in the present work we are interested in finding $J_n(A,S)$ for small values of X and the corresponding expression is given by

$$J_n(A,S) \approx \sqrt{\pi} S^n \left[1 + \frac{n-1}{2} X + \left\{ \frac{n}{2}\left(\frac{n}{4} - 1\right) + \frac{21}{16} \right\} X^2 + ... \right] e^{-A/S} \tag{43}$$

Small positive S

For small values of S, the expression for $J_n(A,S)$ is given by

$$J_n(A,S) = (1 - S^2) J_n(A,0) + 2S J_{n+1}(A,0) + 2S^2 J_{n+2}(A,0) + O(S^3) \tag{44}$$

where the expansions for the function $J_n(A,0)$ are given by the eq.s (41) and (42).

Negative S

For small negative S, the expansion for $J_n(A,S)$ given by the eq. (44) is still valid with due regard to the sign of S. However, for large negative values of S the values of $J_n(A,S)$ are too small and can be neglected.

We observe that, the evaluation of the split fluxes using the above expressions is expensive as it involves a lot of computations. Also, there will be a loss in accuracy due to these expressions, which are accurate upto two decimal places for some range of values of A and S. However, more accurate formulae can be derived but computationally they will be expensive.

3.3.2 The second model, $\phi = e^{-\alpha|v|}$:

In this case the expressions for the split fluxes are given by

$$Gm^{\pm} = \left\langle \Psi, \frac{v \pm |v| e^{-\alpha|v|}}{2} F \right\rangle \tag{45}$$

$$= \int\limits_{\mathbb{R}^+ \times \mathbb{R}} \Psi \frac{v \pm |v| e^{-\alpha|v|}}{2} F \, dv dI \tag{46}$$

After performing integrations, the closed form expressions for the split fluxes are given by

$$Gm^{\pm} = \frac{G}{2} \pm \frac{1}{2}\left[e^{\left(\frac{\alpha^2}{4\beta}-\alpha u\right)} G^{+}\left(u - \frac{\alpha}{2\beta}\right) - e^{\left(\frac{\alpha^2}{4\beta}+\alpha u\right)} G^{-}\left(u + \frac{\alpha}{2\beta}\right)\right] \tag{47}$$

where G is the unsplit flux, $G^{\pm}$ are the usual *kfvs* split fluxes for the $1D$ Euler equations. Note that, these expressions are simpler as they are similar to that of *kfvs* split fluxes, except that the arguments of error function and exponentials are different. Computationally, the evaluation of these fluxes take the same amount of time as that of *kfvs* split fluxes, except that it involves the evaluation of one more error function.

4 Numerical scheme based on m-kfvs

In this section we derive a finite volume method based on *m-kfvs* for the $1D$ Euler equations. Consider the $1D$ Boltzmann equation given by (2)

$$\frac{\partial F}{\partial t} + \frac{\partial (vF)}{\partial x} = 0$$

A finite volume based discretisation of the space derivative at the point j on a three point stencil $\{j-1, j, j+1\}$ gives the semi-discretized equation [11]

$$\Delta x \left(\frac{\partial F}{\partial t}\right)_j^n + \left[(vF)_{j+\frac{1}{2}} - (vF)_{j-\frac{1}{2}}\right]^n = 0 \tag{48}$$

Introducing upwind bias by splitting the molecular velocity v into v^+ and v^- using the MCIR splitting, we have

$$\Delta x \left(\frac{\partial F}{\partial t}\right)_j^n + \left[(v^+F)_{j+\frac{1}{2}} - (v^+F)_{j-\frac{1}{2}}\right]^n + \left[(v^-F)_{j+\frac{1}{2}} - (v^-F)_{j-\frac{1}{2}}\right]^n = 0 \tag{49}$$

where $v^{\pm} = \frac{v \pm |v|\phi}{2}$, ϕ is a dissipation control function as defined in the eq. (24). Using a constant in a cell approximation, the cell interface values are given by

$$F_{j+\frac{1}{2}} = \begin{cases} F_j & \text{if } v > 0 \\ F_{j+1} & \text{if } v < 0 \end{cases} \qquad F_{j-\frac{1}{2}} = \begin{cases} F_{j-1} & \text{if } v > 0 \\ F_j & \text{if } v < 0 \end{cases}$$

Using the above defined cell interface values eq. (49) reduces to

$$\Delta x \left(\frac{\partial F}{\partial t}\right)_j^n + \left[(v^+F)_j - (v^+F)_{j-1}\right]^n + \left[(v^-F)_{j+1} - (v^-F)_j\right]^n = 0 \tag{50}$$

Replacing the time derivative by a forward difference approximation and taking the Ψ - moments, we get

$$U_j^{n+1} = U_j^n + \frac{\Delta t}{\Delta x}\left[\left\{(Gm^+)_j - (Gm^+)_{j-1}\right\}^n + \left\{(Gm^-)_{j+1} - (Gm^-)_j\right\}^n\right] \tag{51}$$

which is an upwind scheme for the $1D$ Euler equations based on *m-kfvs* method and $Gm^{\pm}$ are the corresponding split fluxes and are derived in section (3.3). It can be easily shown that the above scheme is generally first order accurate in space and time. However, the dissipation in the numerical scheme can be controlled by choosing proper value of α, as the modified split fluxes $Gm^{\pm}$ are nonlinear functions of parameter α. We now choose values of α for both the models. Some case is required in choice of α to ensure conservation.

Conservation of scheme (51) is ensured if $G_{j+\frac{1}{2}} = Gm_j^+ + Gm_{j+1}^-$ cancels when two cells C_j and C_{j+1} are considered together. This condition implies that $G_{j+\frac{1}{2}}$ appearing in state update of cell j must be equal to $G_{j+\frac{1}{2}}$ appearing in state update of cell C_{j+1}. Hence there must be only one value of α_j at each j. This is best ensured by specifying

$$\alpha_j = \begin{cases} \tilde{\alpha}_d/\sqrt{\beta_r}, & \text{for } \phi = e^{-\frac{\alpha}{|v|}} \\ \tilde{\alpha}_d\sqrt{\beta_r}, & \text{for } \phi = e^{-\alpha|v|} \end{cases} \tag{52}$$

where suffix d stands for discontinuous region and β_r is reference value of β. In regions of smooth variation, we specify

$$\alpha_j = \begin{cases} \tilde{\alpha}_s/\sqrt{\beta_r}, & \text{for } \phi = e^{-\frac{\alpha}{|v|}} \\ \tilde{\alpha}_s\sqrt{\beta_r}, & \text{for } \phi = e^{-\alpha|v|} \end{cases} \tag{53}$$

A sensor is required to decide when $\tilde{\alpha} = \tilde{\alpha}_d$ and $\tilde{\alpha} = \tilde{\alpha}_s$. In the present work we have used a sensor based on directed divergence [13] between two Maxwellian distributions, commonly known as Mahalanobis distance or D^2 distance[1] [9, 20]. The D^2 distance between two Maxwellians is given by

$$\begin{aligned} D^2\left(F_i, F_j\right) = &\left(\rho_j - \rho_i\right) \ln\left[\frac{\rho_i}{\rho_j}\left(\frac{T_i}{T_j}\right)^{\frac{5}{2}}\right] + \frac{\rho_i}{2RT_i}\left[\frac{\rho_j}{\rho_i} + \frac{T_i}{T_j}\right]\left(u_i - u_j\right)^2 \\ &+ \frac{5}{2}\left[\frac{\rho_i\left(T_i - T_j\right)}{T_j} + \frac{\rho_i\left(T_i - T_j\right)}{T_j}\right] \end{aligned} \tag{54}$$

We now define the sensor function S_j as

$$S_j = \frac{Max\left\{\frac{D^2(F_j,F_{j-1})}{\Delta x^2_{j-\frac{1}{2}}}, \frac{D^2(F_j,F_{j+1})}{\Delta x^2_{j+\frac{1}{2}}}\right\}}{Min\left\{\frac{D^2(F_j,F_{j-1})}{\Delta x^2_{j-\frac{1}{2}}}, \frac{D^2(F_j,F_{j+1})}{\Delta x^2_{j+\frac{1}{2}}}\right\}} \tag{55}$$

where $\Delta x_{j\pm\frac{1}{2}} = x_{j\pm1} - x_j$. If the value of $S_j > \epsilon$(some specified value), then there exists a discontinuity between points $\{j-1,\ j,\ j+1\}$. In this case we take the value of $\tilde{\alpha}$ to be $\tilde{\alpha}_d$.

[1]It is not a metric distance. It does not satisfy the triangular inequality.

$S_j < \epsilon$ denotes a smooth region and we define $\tilde{\alpha}$ to be $\tilde{\alpha}_s$. It may be noted that ϵ is a constant and needs to be specified by the user. Near the discontinuity the value of $\tilde{\alpha}_d$ is chosen in such a way that the solution is non-oscillatory and discontinuties are not unduly smeared. In smooth regions, a high value of $\tilde{\alpha}$ ($\tilde{\alpha}_s \geq \tilde{\alpha}_d$) is chosen so that we can obtain near second order accuracy.

5 Results and Discussion

Here we illustrate the performance of *m-kfvs* method by applying it to standard test cases for one-dimensional flows. Numerical solutions are compared with the results obtained using first order accurate *kfvs* method and exact solution.

5.1 Shock tube problem:

The initial conditions are chosen with a pressure jump of 2 across the shock. Numerical solutions are performed on the computational domain $0 \leq x \leq 1$ with 500 equally spaced cells.

Figs. 3 and 4 show the results obtained using *m-kfvs* method with $\phi = e^{-\frac{\alpha}{|v|}}$ and $\phi = e^{-\alpha|v|}$ respectively. It has been observed that the *m-kfvs* method captures the discontinuties more crisply compared to the usual first order accurate *kfvs* method and very good accuracy is achieved in smooth regions. Figs. 3(c) and 4(c) show the variation in $\tilde{\alpha}$ after the final solution.

When large values of $\tilde{\alpha}$ are employed at all grid points, the discontinuties are captured more sharply and excellent accuracy is achieved in smooth regions. But the monotonicity is lost as there are spurious oscillations developing in the viscinity of the shock and is shown in Figs. 5 and 6. Also, we observe some oscillations near the expansion using the model $\phi = e^{-\frac{\alpha}{|v|}}$. The numerical simulations show that by choosing proper $\tilde{\alpha}$ we can control the dissipation which in turn controls accuracy and oscillations.

5.2 Convergent-divergent nozzle problem:

The *m-kfvs* scheme has been applied to a convergent-divergent nozzle problem [12]. This is a steady state test case with flow being quasi-one-dimensional, inviscid and compressible. The results are compared with *kfvs*, second order accurate *MacCormack* scheme [12] and the exact solution.

We briefly explain the governing equations, corresponding velocity distribution function and the split fluxes for the *m-kfvs* method.

The governing equations of the quasi-one-dimensional flow are given by

$$\frac{\partial U}{\partial t} + \frac{\partial Gx}{\partial x} = S \tag{56}$$

Where U is the vector of conserved variables, Gx is the flux vector along x-direction and S is the source term vector, given by

$$U = \begin{bmatrix} \rho A \\ \rho u A \\ \rho e A \end{bmatrix}, \quad G = \begin{bmatrix} \rho u A \\ (p + \rho u^2) A \\ (p + \rho e) A \end{bmatrix} \quad and \quad S = \begin{bmatrix} 0 \\ p \frac{dA}{dx} \\ 0 \end{bmatrix} \tag{57}$$

where ρ density, u fluid velocity along x-direction, e total energy, p pressure and A cross-sectional area of the nozzle, $A = A(x)$. Using the Operator splitting **??**, the system of equations given by (56) can be rewritten as

$$\frac{\partial U}{\partial t} + \frac{\partial Gx}{\partial x} = 0 \tag{58}$$

$$\frac{\partial U}{\partial t} = S \tag{59}$$

Note that, the eq. (58) can be obtained by taking the Ψ - moments of the $1D$ Boltzmann equation (2) with the velocity distribution function given by

$$F = A \frac{\rho}{I_0} \sqrt{\frac{\beta}{\pi}} e^{-\beta(v-u)^2 - I/I_0} \tag{60}$$

The state update formula for the system of equations (56) is given by

$$U_j^{n+1} = U_j^{*n} - \frac{\Delta t}{\Delta x} \left[\left\{ (Gmx^+)_j + (Gmx^-)_{j+1} \right\}^n - \left\{ (Gmx^+)_{j-1} + (Gmx^-)_j \right\}^n \right] \tag{61}$$

Here, $Gmx^{\pm}$ are the *m-kfvs* split fluxes for the quasi-one-dimensional problem and the corresponding expressions are given by $Gmx^{\pm} = A\, Gm^{\pm}$, where $Gm^{\pm}$ are the *m-kfvs* split fluxes for the $1D$ Euler equations and $U^* = U + \begin{bmatrix} 0 & p\frac{dA}{dx}\Delta t & 0 \end{bmatrix}^T$.

The initial conditions are chosen in such a way that there exists a steady normal shock in the divergent portion of the nozzle. The non-dimensional values of the initial conditions are given by

$$\left.\begin{aligned} \rho' &= 1.0 \\ T' &= 1.0 \end{aligned}\right\} \quad \text{for } 0 \le x' \le 0.5$$

$$\left.\begin{aligned} \rho' &= 1.0 - 0.366(x' - 0.5) \\ T' &= 1.0 - 0.167(x' - 0.5) \end{aligned}\right\} \quad \text{for } 0.5 \le x' \le 1.5$$

$$\left.\begin{aligned}\rho' &= 0.634 - 0.702(x' - 1.5)\\ T' &= 0.833 - 0.4908(x' - 1.5)\end{aligned}\right\} \quad \text{for } 1.5 \le x' \le 2.1$$

$$\left.\begin{aligned}\rho' &= 0.5892 + 0.10228(x' - 2.1)\\ T' &= 0.93968 + 0.0622(x' - 2.1)\end{aligned}\right\} \quad \text{for } 2.1 \le x' \le 3.0$$

$$u' = \frac{0.59}{\rho' A'}$$

and the cross-sectional area of the nozzle is given by

$$A' = 1.0 + 2.2(x' - 1.5)^2, \quad 0 \le x' \le 3.$$

Numerical simulations are performed on a uniform grid with 61 cells. Figs. 7(a) and 8(a) show the pressure distribution through the nozzle. It has been observed that the *m-kfvs* scheme is less dissipative and captures the shock more accurately when compared to *kfvs*. The computed results are in very good agreement with well-known second order accurate MacCormack scheme. Figs. 7(b) and 8(b) show the corresponding variation in $\tilde{\alpha}$.

Convergence history of residual:

We show the another important aspect of the *m-kfvs* scheme, namely the residual convergence rate. The L_2 norm of the residue is calculated and is plotted against the number of iterations for the convergent divergent nozzle problem. Figs. 7(c) and 8(c) show that the residue continues to decrease to machine zero as similar to the case of *kfvs* scheme. However, the convergence rate depends on the value of $\tilde{\alpha}$. It also must be emphasized that (well-known in CFD) higher fall in residue does not imply more accurate solution!

6 Conclusions and future study

The *m-kfvs* method based on MCIR splitting with dissipation control functions $\phi = e^{-\frac{\alpha}{|v|}}$ or $\phi = e^{-\alpha|v|}$ capture the discontinuties more sharply and very good accuracy is achieved in smooth regions. By tuning α, we can obtain nearly second order accuracy in smooth regions and can sharply resolve the discontinuties without spurious oscillations. The convergence behaviour of the residual is as good as the first order accurate *kfvs* scheme. The model $\phi = e^{-\alpha|v|}$ is preferred as closed form expressions for the split fluxes can be obtained and these are simpler. In the case of $\phi = e^{-\frac{\alpha}{|v|}}$, there will be some loss in accuracy due to the series and asymptotic expansions. Infact, computationally, the *m-kfvs* method based on the model $\phi = e^{-\alpha|v|}$ is almost as fast as *kfvs* method except that it involves the evaluation of one more error function in the expressions for the split fluxes. The choice $\phi = e^{-\frac{\alpha}{|v|}}$ is computationally more expensive as it involves a lot

of computations.

The MCIR idea can be easily extended to higher dimensions. Infact, the potential value addition of the above idea to existing finite volume or grid free codes based on *kfvs* is immense. Just by changing the expressions for the split fluxes in the flux calculation subroutine will yield *m-kfvs* based codes having less numerical disipation, resulting in accurate capture of leading edge suction, crisp shocks, negligible loss of stagnation pressure in isentropic regions and accurate prediction of vortex dominated flows. Some more mathematical analysis and numerical experiments are obviously required to find the optimal value of α.

Acknowledgements

I sincerely thank Praveen, Mohan Varma and Ram Palekar for many helpful discussions and kind help. Thanks are due to Dr. V. Ramesh for his constant encouragement and discussions. I also wish to acknowledge Miss. Nagarathna for providing promptly Prof. R. Narasimha's papers.

Appendix A

kfvs split fluxes in one dimension:

The *kfvs* split flux expressions for the $1D$ Euler equations are given by

$$G^{\pm} = \begin{bmatrix} \rho u A^{\pm} \pm \frac{\rho}{\sqrt{\pi\beta}} B \\ (p + \rho u^2) A^{\pm} \pm \frac{\rho u}{\sqrt{\pi\beta}} B \\ (p + \rho e) u A^{\pm} \pm \frac{\rho}{\sqrt{\pi\beta}} (\frac{p}{2\rho} + e) B \end{bmatrix} \tag{62}$$

where

$$A^{\pm} = \frac{1 \pm erf(s)}{2}, \quad B = \frac{e^{-s^2}}{2} \quad \text{and} \quad s = u\sqrt{\beta}.$$

m-kfvs split fluxes in two dimensions:

In this section we derive the expressions for the split fluxes for $2D$ Euler equations using *m-kfvs* method. Let us consider the 2D Boltzmann equation in the Euler limit

$$\frac{\partial F}{\partial t} + \frac{\partial}{\partial x}(v_1 F) + \frac{\partial}{\partial x}(v_2 F) = 0 \tag{63}$$

where v_1, v_2 are molecular velocities along x and y directions respectively and F is the Maxwellian velocity distribution function, in the case of two dimensions it is given by

$$F = \frac{\rho}{I_0} \frac{\beta}{\pi} e^{-\beta \left[(v_1 - u_1)^2 + (v_2 - u_2)^2 \right] - I/I_0} \tag{64}$$

Using the MCIR splitting, eq. (63) gives the MCIR-split Boltzmann equation

$$\frac{\partial F}{\partial t} + \frac{\partial}{\partial x}(v_1^+ F) + \frac{\partial}{\partial x}(v_1^- F) + \frac{\partial}{\partial y}(v_2^+ F) + \frac{\partial}{\partial y}(v_2^- F) = 0 \tag{65}$$

where

$$v_i^{\pm} = \frac{v_i \pm |v_i|\phi_i}{2},\ i = 1, 2.$$

Here, ϕ_1 and ϕ_2 are dissipation control fuctions along x and y directions respectively. For ϕ, we have chosen the model $\phi = e^{-\alpha|v|}$ as the closed form expressions for the split fluxes are simpler. Taking the Ψ - moments [14] of eq. (65), we obtain the modified *kfvs* Euler equations in two dimensions,

$$\frac{\partial U}{\partial t} + \frac{\partial Gxm^+}{\partial x} + \frac{\partial Gxm^-}{\partial x} + \frac{\partial Gym^+}{\partial y} + \frac{\partial Gym^-}{\partial y} = 0 \tag{66}$$

where $Gxm^{\pm}$ and $Gym^{\pm}$ are the split fluxes along x and y directions respectively, given by

$$Gxm^{\pm} = \left\langle \Psi,\ \frac{v_1 \pm |v_1|\phi_1}{2} F \right\rangle = \int\limits_{\mathbb{R}^+ \times \mathbb{R}^2} \Psi \frac{v_1 \pm |v_1|\phi_1}{2} F dv_1 dv_2 dI \tag{67}$$

$$Gym^{\pm} = \left\langle \Psi,\ \frac{v_2 \pm |v_2|\phi_2}{2} F \right\rangle = \int\limits_{\mathbb{R}^+ \times \mathbb{R}^2} \Psi \frac{v_2 \pm |v_2|\phi_2}{2} F dv_2 dv_1 dI \tag{68}$$

On performing integrations, the closed form expressions for the split fluxes are given by

$$Gxm^{\pm} = \frac{Gx}{2} \pm \frac{1}{2}\left[e^{\left(\frac{\alpha_1^2}{4\beta} - \alpha_1 u_1\right)} Gx^+\left(u_1 - \frac{\alpha_1}{2\beta}\right) - e^{\left(\frac{\alpha_1^2}{4\beta} + \alpha_1 u_1\right)} Gx^-\left(u_1 + \frac{\alpha_1}{2\beta}\right) \right] \tag{69}$$

$$Gym^{\pm} = \frac{Gy}{2} \pm \frac{1}{2}\left[e^{\left(\frac{\alpha_2^2}{4\beta} - \alpha_2 u_2\right)} Gy^+\left(u_2 - \frac{\alpha_2}{2\beta}\right) - e^{\left(\frac{\alpha_2^2}{4\beta} + \alpha_2 u_2\right)} Gy^-\left(u_2 + \frac{\alpha_2}{2\beta}\right) \right] \tag{70}$$

where Gx and Gy are unsplit fluxes, $Gx^{\pm}$ and $Gy^{\pm}$ are the usual *kfvs* split fluxes [14] along x and y directions respectively. Here, α_1 and α_2 are parameters through which we can control the numerical dissipation. Note that, in the limit $\alpha_1, \alpha_2 \to 0$, the above equations give the *kfvs* split fluxes for the $2D$ Euler equations.

Split fluxes for m-kfvs in three dimensions:

Proceeding in the lines of $1D$ and $2D$, the *m-kfvs* split Euler equations in three dimensions are given by

$$\frac{\partial U}{\partial t} + \frac{\partial Gxm^+}{\partial x} + \frac{\partial Gxm^-}{\partial x} + \frac{\partial Gym^+}{\partial y} + \frac{\partial Gym^-}{\partial y} + \frac{\partial Gzm^+}{\partial z} + \frac{\partial Gzm^-}{\partial z} = 0 \tag{71}$$

where $Gxm^{\pm}$, $Gym^{\pm}$ and $Gzm^{\pm}$ are the *m-kfvs* split fluxes along x, y and z directions respectively, and are given by

$$Gxm^{\pm} = \left\langle \Psi, \frac{v_1 \pm |v_1|\phi_1}{2} F \right\rangle = \int\limits_{\mathbb{R}^+ \times \mathbb{R}^3} \Psi \frac{v_1 \pm |v_1|\phi_1}{2} F dv_1 dv_2 dv_3 dI \tag{72}$$

$$Gym^{\pm} = \left\langle \Psi, \frac{v_2 \pm |v_2|\phi_2}{2} F \right\rangle = \int\limits_{\mathbb{R}^+ \times \mathbb{R}^3} \Psi \frac{v_2 \pm |v_2|\phi_2}{2} F dv_2 dv_1 dv_3 dI \tag{73}$$

$$Gzm^{\pm} = \left\langle \Psi, \frac{v_3 \pm |v_3|\phi_3}{2} F \right\rangle = \int\limits_{\mathbb{R}^+ \times \mathbb{R}^3} \Psi \frac{v_3 \pm |v_3|\phi_3}{2} F dv_3 dv_1 dv_2 dI \tag{74}$$

where $\phi_i = e^{-\alpha_i |v_i|}$, $i = 1, 2, 3$. On performing the respective integrations, the closed form expressions for the split fluxes in $3D$ are given by

$$Gxm^{\pm} = \frac{Gx}{2} \pm \frac{1}{2}\left[e^{\left(\frac{\alpha_1^2}{4\beta} - \alpha_1 u_1\right)} Gx^{+}\left(u_1 - \frac{\alpha_1}{2\beta}\right) - e^{\left(\frac{\alpha_1^2}{4\beta} + \alpha_1 u_1\right)} Gx^{-}\left(u_1 + \frac{\alpha_1}{2\beta}\right) \right] \tag{75}$$

$$Gym^{\pm} = \frac{Gy}{2} \pm \frac{1}{2}\left[e^{\left(\frac{\alpha_2^2}{4\beta} - \alpha_2 u_2\right)} Gy^{+}\left(u_2 - \frac{\alpha_2}{2\beta}\right) - e^{\left(\frac{\alpha_2^2}{4\beta} + \alpha_2 u_2\right)} Gy^{-}\left(u_2 + \frac{\alpha_2}{2\beta}\right) \right] \tag{76}$$

$$Gzm^{\pm} = \frac{Gz}{2} \pm \frac{1}{2}\left[e^{\left(\frac{\alpha_3^2}{4\beta} - \alpha_3 u_3\right)} Gz^{+}\left(u_3 - \frac{\alpha_3}{2\beta}\right) - e^{\left(\frac{\alpha_3^2}{4\beta} + \alpha_3 u_3\right)} Gz^{-}\left(u_3 + \frac{\alpha_3}{2\beta}\right) \right] \tag{77}$$

where Gx, Gy and Gz are unsplit fluxes, $Gx^{\pm}$, $Gy^{\pm}$ and $Gz^{\pm}$ are the *kfvs* split fluxes [24] along x, y and z coordinate directions respectively. Also $u_i^{\pm} = u_i \mp \frac{\alpha_i}{2\beta}$, $i = 1, 2, 3$. In the case of $3D$, we have three parameters α_1, α_2 and α_3 through which we can control the numerical dissipation. Note that, in the limit $\alpha_i \to 0$, $i = 1, 2, 3$, the modified split fluxes given by eq.s (75), (76) and (77) reduce to the usual *kfvs* split fluxes in three dimensions.

References

[1] Abramowitz M. Evaluation of the integral $\int\limits_0^{\infty} e^{-u^2 - x/u} du$. *J. Math. and Phys.*, 32, 188, 1953.

[2] Mahendra A.K. Application of least squares kinetic upwind method to strongly rotating viscous flows. *M.Sc. (Engg.) Thesis*, Dept. of Aerospace Engg., IISc, Bangalore, India, 2003.

[3] Anandhanarayanan K. Development and applications of a gridfree kinetic upwind solver to multibody configurations. *Ph.D. Thesis*, Dept. of Aerospace Engg., IISc, Bangalore, India, 2003.

[4] Chahine M.T. and Narasimha R. The integral $\int\limits_0^{\infty} v^n e^{-(v-u)^2 - \frac{x}{v}} dv$. *J. Math. Phys.*, 43, 163, 1964.

[5] Courant R., Isaacson E. and Rees M. On the solution of Nonlinear Hyperbolic Differential Equations by Finite Differences. *Comm. Pure Appl. Math.*, 5, 243-255, 1952.

[6] Deshpande S.M. Kinetic flux splitting schemes. *Computational Fluid Dynamics Review 1995*, (eds.) M.M. Hafez and K. Oshima, John Wiley & Sons Ltd., 1995.

[7] Deshpande S.M. A second order accurate Kinetic Theory based method for inviscid compressible flows. *NASA Technical Paper 2613*, NASA Langely Research Centre, Hampton, Virginia, 1986.

[8] Dominic John Chander. A One Point Shock Capturing Kinetic Scheme for Hyperbolic Conservation Laws. *M.E. Thesis*, Dept. of Aerospace Engg., IISc, Bangalore, India, 2004.

[9] Ghosh A.K. Robust Least Squares Kinetic Upwind Method for inviscid compressible flows. *Ph.D. Thesis*, Dept. of Aerospace Engg., IISc, Bangalore, India, 1996.

[10] Jaisankar S. and Raghurama Rao S.V. A Low Dissipative Peculiar Velocity Based Upwind Method. 7^{th} *AeSI CFD symposium*, August 2004, Bangalore, India.

[11] Jameson A. Analysis and design of numerical schemes for gas dynamics 1, artificial diffusion, upwind biasing, limiters and their effect on multigrid convergence. *RIACS Technical Report No. 94.15, Int. J. of Comp. Fluid Dymanics*, 4, 171-218, 1995.

[12] John D. Anderson Jr. Computational Fluid Dynamics - The Basics with Applications. *McGraw Hill International Editions.*

[13] Kullback S. Information Theory and Statistics. *Dover Publications, Inc.*, New York, 1967.

[14] Mandal J.C. Kinetic Upwind Method for Inviscid Compressible Flows. *Ph.D. Thesis*, Dept. of Aerospace Engg., IISc, Bangalore, India, 1989.

[15] Perthame Benoit. Kinetic Formulation of Conservation Laws. *Oxford lecture series in mathematics and applications*, Dec. 2002.

[16] Prendergast K.H. and Kun Xu. Numerical Hydrodynamics frm Gas Kinetic Theory. *J. of Comp. Phys.*, 109, 53, 1993.

[17] Praveen C. and Deshpande S.M. Kinetic Meshless Method. *Report 2003 FM 10*, Dept. of Aerospace Engg., IISc, Bangalore, India.

[18] Praveen C. Least Squares Based Kinetic Schemes for Euler Equations. *Ph.D. Thesis*, Dept. of Aerospace Engg., IISc, Bangalore, India, 2004.

[19] Pullin D. Direct Simulation Methods for Compressible Inviscid Ideal Gas Flow. *J. Comp. Phys.*, 34, 231, 1980.

[20] Raghavendra N.V., Mohan Varma, Biju Uthup and Deshpande S.M. 3-D Grid Adaptation using a Sensor based on Directed Divergence between Maxwellians. 1^{st} *ICCFD*, Japan, July, 2000.

[21] Raghurama Rao S.V. and Deshpande S.M. Peculiar Velocity based Upwind Method for Inviscid Compressible Flows. *J. of Comp. Fluid Dynamics*, 3, 415-432, 1994.

[22] Ramesh V. and Deshpande S.M. Least squares kinetic upwind method with modified CIR splitting. 7^{th} *AeSI CFD symposium*, August 2004, Bangalore, India.

[23] Ramesh V. and Deshpande S.M. Low dissipation grid free upwind kinetic scheme with modified CIR splitting. *Report 2004 FM 20*, Dept. of Aerospace Engg., IISc, Bangalore, India.

[24] Ramesh V. Least Squares Grid Free Kinetic Upwind Method. *Ph.D. Thesis*, Dept. of Aerospace Engg., IISc, Bangalore, India, 2001.

[25] Sanders R.H. and Prendergast K.H. The possible relation of the three-kiloparsec arm to explosions in the galactic nucleus. *Astrophysical Journal*, 188, 1974.

[26] Sekar S., Nagarathinam M., Deshpande S.M. Kinetic surface transpiration with KFVS Euler code for treating control curface deflection. *Proceedings of the* 6^{th} *Asian Congress of Fluid Mechanics*, Singapore, May 22-26, 1995.

[27] Strang G., On the construction and comparison of difference schemes. *SIAM J. Numer. Anal.*, vol. 5, 1968, p. 506-517.

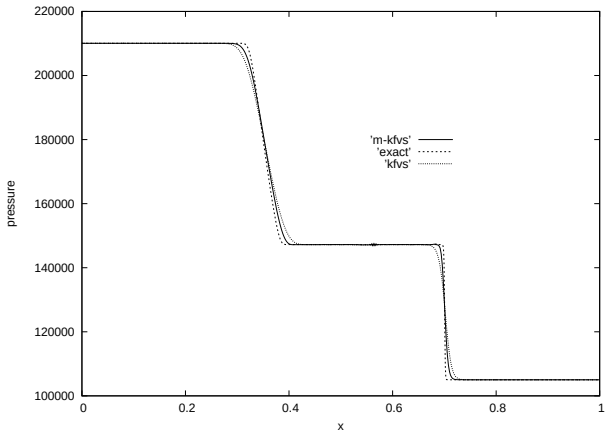

(a) Pressure plot

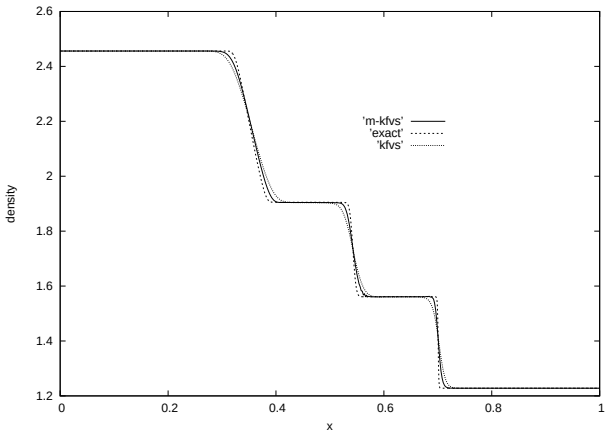

(b) Density plot

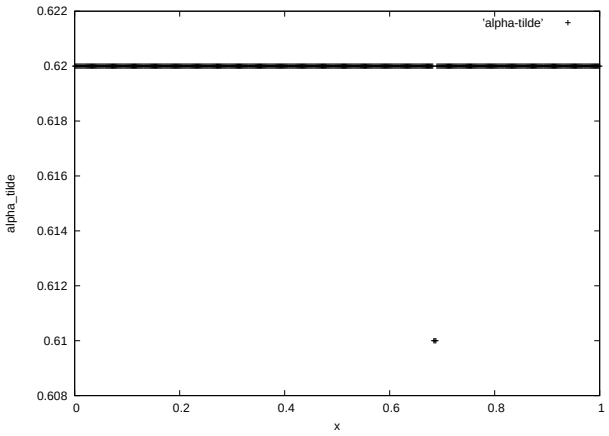

(c) Variation of $\tilde{\alpha}$

Figure 3: Shock tube problem using *m-kfvs* with $\phi = e^{-\frac{\alpha}{|v|}}$. Computed results are compared with first order *kfvs* scheme and exact solution.

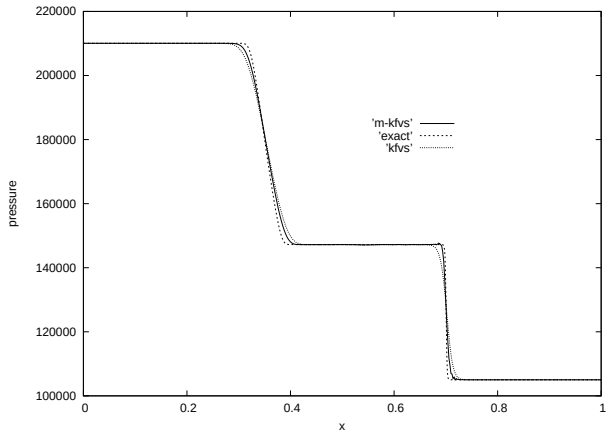

(a) Pressure plot

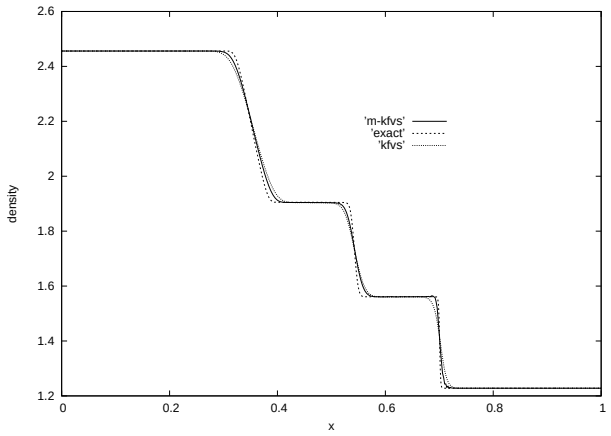

(b) Density plot

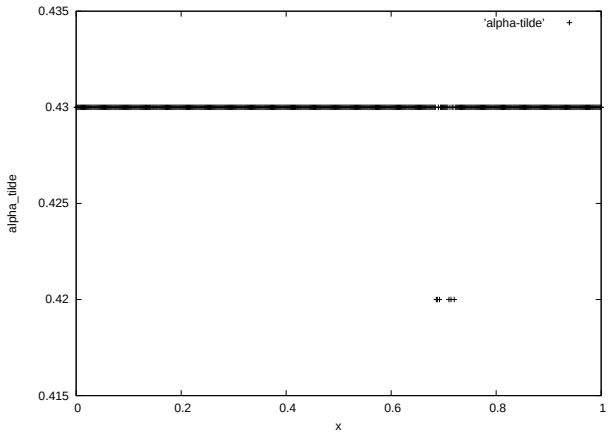

(c) Variation of $\tilde{\alpha}$

Figure 4: Shock tube problem using *m-kfvs* with $\phi = e^{-\alpha|v|}$. Computed results are compared with first order *kfvs* scheme and exact solution.

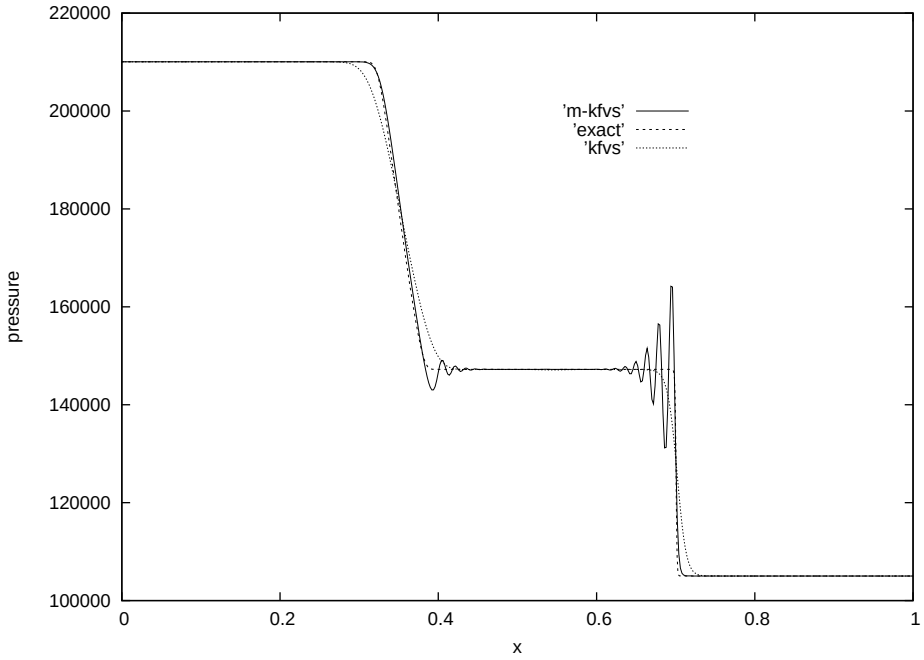

(a) Pressure plot

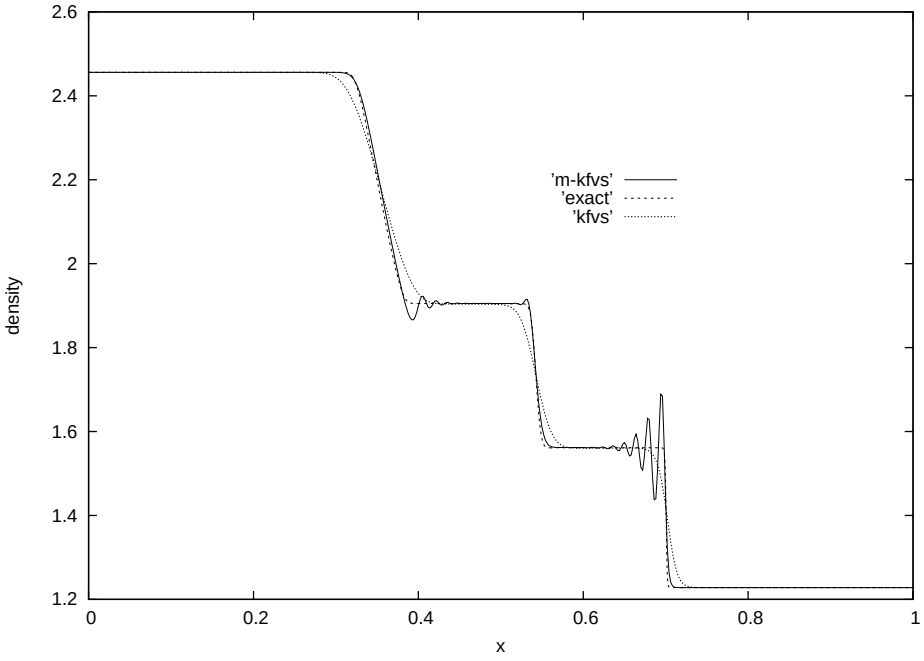

(b) Density plot

Figure 5: Shock tube problem using *m-kfvs* with $\phi = e^{-\frac{\alpha}{|v|}}$. Numerical solution for large value of $\tilde{\alpha}$, $\tilde{\alpha}_d = \tilde{\alpha}_s = 1.8$.

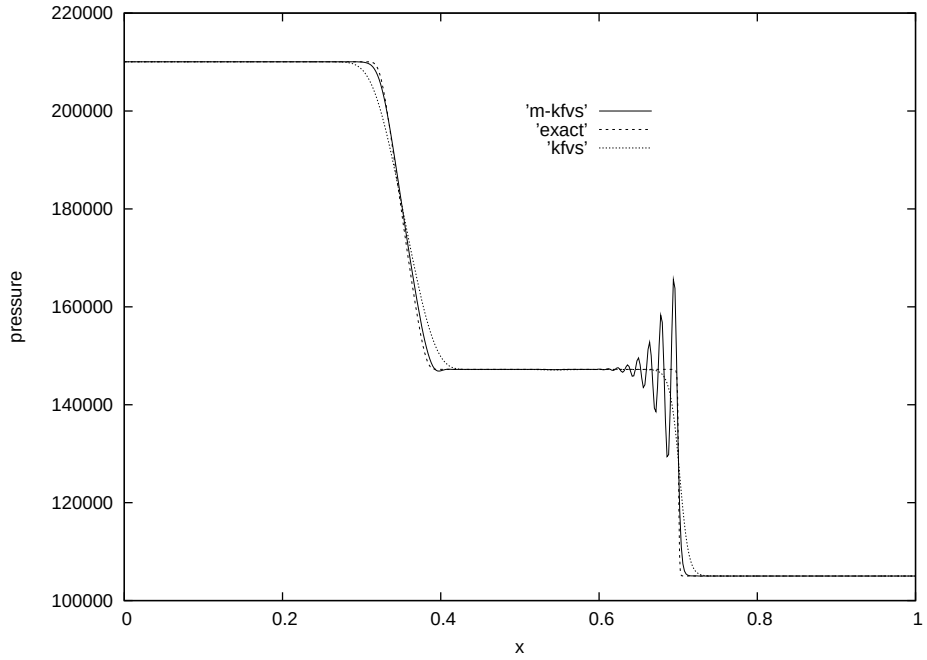

(a) Pressure plot

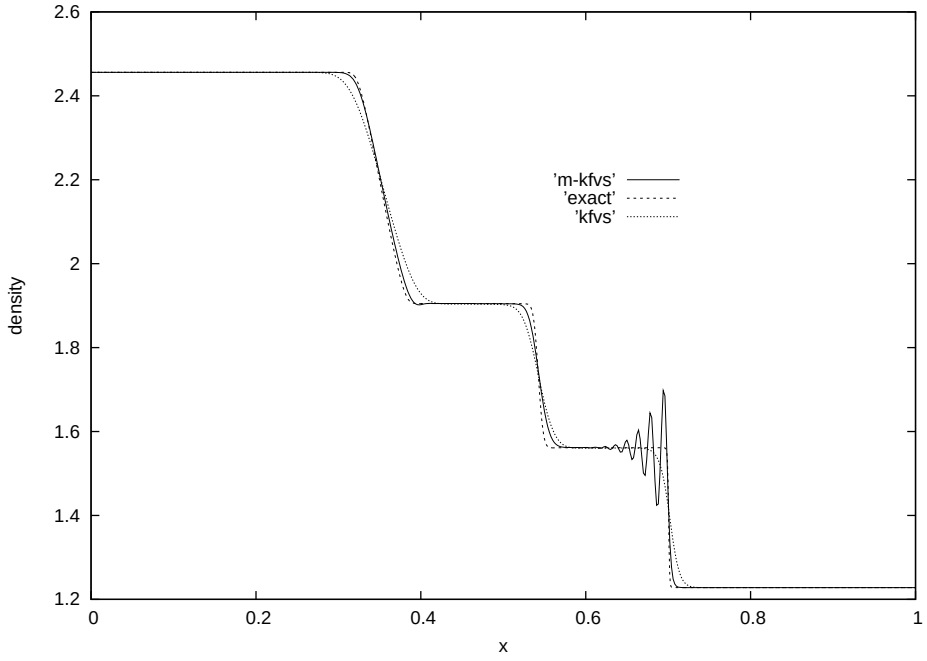

(b) Density plot

Figure 6: Shock tube problem using *m-kfvs* with $\phi = e^{-\alpha|v|}$. Numerical solution for large value of $\tilde{\alpha}$, $\tilde{\alpha}_d = \tilde{\alpha}_s = 1.0$.

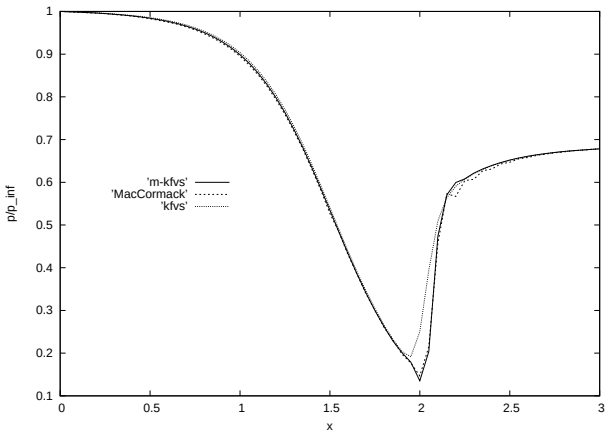

(a) Pressure distribution through the nozzle

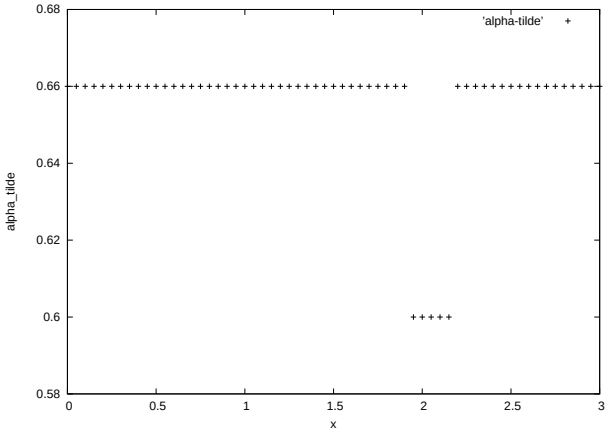

(b) Variation of $\tilde{\alpha}$

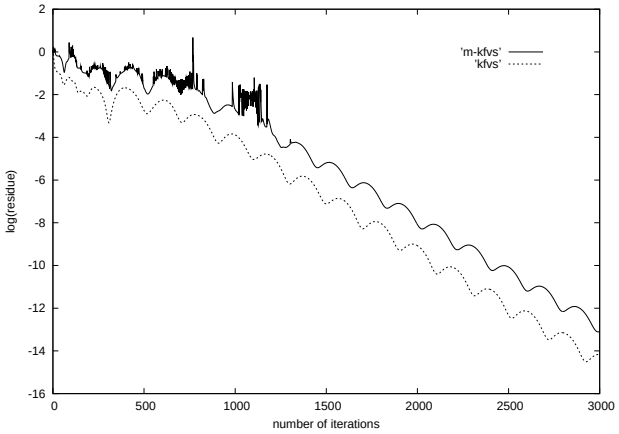

(c) Convergence history

Figure 7: Convergent divergent nozzle problem using the model $\alpha = e^{-\frac{\alpha}{|v|}}$. Computed results are compared with first order *kfvs* and second order MacCormack schemes.

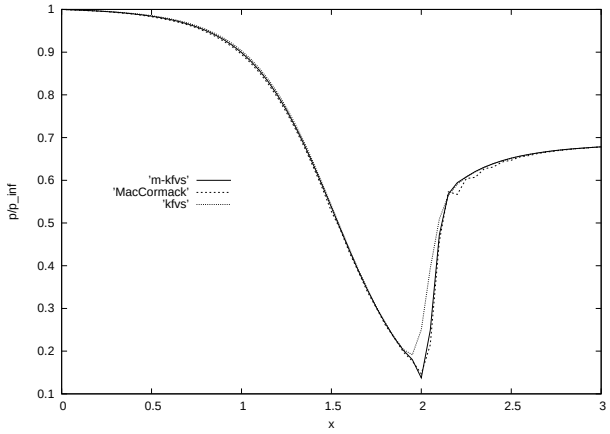

(a) Pressure distribution through the nozzle

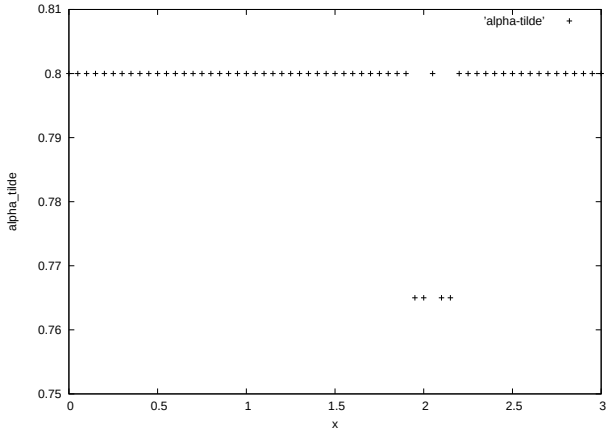

(b) Variation of $\tilde{\alpha}$

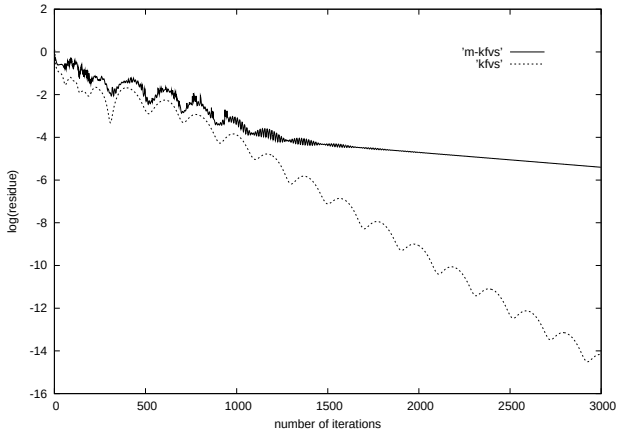

(c) Convergence history

Figure 8: Convergent divergent nozzle problem using the model $\alpha = e^{-\alpha|v|}$. Computed results are compared with first order *kfvs* and second order MacCormack schemes.